Dynamic Vibration Modelling and Damping Optimisation of a Combine Harvester Cutter System Using Cuckoo Search Algorithm

Kuizhou Ji, Yaoming Li, Yuhang Chen, Yanbin Liu, Hanhao Wang and Zhiwu Yu

School of Agricultural Engineering, Jiangsu University, Zhenjiang 212013, China.
Key Laboratory of Modern Agricultural Equipment and Technology (Jiangsu University), Ministry of Education, Zhenjiang 212013, China. E-mail: ymli@ujs.edu.cn

(Received 16 October 2024; accepted 23 February 2025)

The goal of this study is to help solve the problem of large vibrations generated by the motion of the cutter and pendulum ring system during the operation of a combined harvester, which in turn leads to significant vibrations in the cab. The kinematic equations of the cutter and pendulum ring system and the simplification of these complex equations into a two-degree-of-freedom system model are established in this study. On this basis, we apply the cuckoo search algorithm to obtain the optimal parameter combination of the cutter system, which can effectively reduce the vibration. The SIMULINK simulation model was constructed to obtain the simulation results of the vibration acceleration of the cutter system under four working conditions. The results prove that the simulation results for Case 1 are similar to the experimental measurements under the original parameters of the harvester. The vibration acceleration amplitude of the cutter is -240 m/s^2 to 220 m/s^2, and the vibration acceleration amplitude of the pendulum ring is -13 m/s^2 to 15 m/s^2, which verifies the correctness of the simplified model and provides a basis for subsequent vibration damping of the cutter system. The experimental study shows that through parameter optimisation and adjustment, the cutter vibration decreased by 8.4% and the cab vibration decreased by 12.9%.

1. INTRODUCTION

Combine harvesters, as complex agricultural machinery, consist of many components with complex motion forms and have numerous excitation parts that generate vibrations. The cutter is one of the important working parts of a combine harvester, which operates on the principle of driving the cutter to perform reciprocating motion to cut crop stalks through a swinging ring mechanism. Under normal working conditions of the harvester, and the cutter together with the swinging ring, generates vibrations that can increase the vibration of the cutting platform. This accelerates the wear of the cutting platform, reducing its service life as well as resulting in excessive vibration in the harvester's cab, affecting the operator's physical and mental health and work status.[1–4] Therefore, the vibration optimisation of the cutter and swinging ring system in combine harvesters is of significant importance for enhancing the service life of the cutting platform and improving the operator's work comfort.[5–8]

In previous research on joint harvest machines, most scholars are more concerned about the structure design, parameter adjustment, and intelligent regulation, so by parts, the motion vibration problem is easy to ignore. There is almost no literature research using some algorithm for vibration reduction optimisation. Even in the latter, operators are more and more interested in their driving comfort and are seeking solutions to some simple vibration reduction measures.

In terms of the harvester cutter, Liu et al.[9] established a kinematic simulation model of a crank linkage cutter and parameterised the push rod length and crank speed of the mechanism. Ran et al.[10] designed a double-action cutter planetary wheel actuator to solve the problem of high vibration of the reciprocating cutter of the traditional oilseed rape combine harvester. Li et al.[11] proposed a simulation and analysis method of grain combine harvester cutter and its whole machine smoothness using ADAMS. Wang et al.[12] took the engine and cutting structure as the research object to solve the vibration problem of the cutting structure of the self-propelled combine harvester, based on the results of force analysis of the cutting structure and the structural dynamics analysis. Pang[13] measured and analysed the time and frequency domain characteristics of the vibration response, which led to the design of a nut with a rubber sleeve to reduce the vibration from the toolbar to the chute. Zhang et al.[14] proposed a vibration control method for a new combined harvester to calculate the optimal combination of weight distribution position and mass to solve the vibration of the cutting structure of a tracked combined harvester. Deng et al.[15] established a mechanical model of the cutter by theoretically analysing the influencing factors of the vibration of the cutter from the dynamic imbalance of the cutting feed system itself in order to explore the dynamic imbalance mechanism of the cutter. Yilmaz et al.[16] used sensors to analyse the noise and vibration of a conventional combine harvester and showed that machine speed and drum speed have a significant effect on the acceleration sensor measurements. Bhandari et al.[17] used Fast Fourier Transform (FFT) with Root Mean Square (RMS) method to evaluate the bearing condition of the threshing drum of the harvesting machine. The fault source identification tool technique was also used to evaluate the looseness, misalignment and imbalance of the combined harvester threshing drum. Titova et al.[18] studied and analysed the non-stationary vibration signals of combine harvester diesel engines, identifying the problem of defective diesel engines connected to the combine harvester through frequency-

Figure 1. Schematic layout of vibration measurement points of combined harvester.

Table 1. Harvester model and acceleration sensor.

Item	Value
Model	YD-186
Working voltage	18-28 V
Working frequency	0.5-5000 kHz
Measuring range	0-500 m/s^2
Sensitivity	10.2 mV/ms^2

apparent local coordinate data.

Most of the research on the vibration of the harvester cutter is to carry out parameter optimisation and structural improvement. However, changing the rotational speed parameters will affect the cutting efficiency at the same time. For example, the reduced speed of the cutter will lead to leakage during crop harvest, and the parameters to be adjusted are not the same for different models, so there is no fundamental solution to the problem of vibration. At present, the method of parameter solution optimisation is not used to improve the cutter system, but in the aspect of the harvester threshing drum, some scholars use the cuckoo algorithm to solve the optimal parameters of the variable diameter threshing drum. To ensure the cutting efficiency of the harvester and reduce vibration at the same time, this paper establishes the kinematic equations of the cutter and the pendulum ring system and then simplifies it into a two-degree-of-freedom system. Through the cuckoo search algorithm, the optimal parameter combinations of the cutter system can be obtained. Thus, the vibration of the cutter system is fundamentally reduced, the service life of the cutting table is improved, and the impact on the driver is reduced as well. It also provides ideas and a basis for simplifying the dynamics model and vibration damping of the subsequent vibrating screen and threshing drum to reduce the vibration of the whole harvester.

2. MATERIALS AND METHODS

2.1. Vibration Acceleration Measurement of Combine Harvester Cutting Table Components

To clarify the correlation of cab vibration caused by the movement of the harvester's cutting table components, Ward's Ruilong premium combine harvester was selected as the test object, and the harvester model was the 4LZ-8.0EZ. The bottom plate of the cutting table, the cab, the left side plate of the cutting table, the right side plate of the cutting table, the cutter, the pendulum ring, the paddle wheel, and the cutting table stirrer were selected as the measurement points.[19–21] The arrangement of the measurement points is shown in Fig. 1.

The vibration acceleration of the arranged measurement points was collected and correlated analysis was conducted through the ZZDASP system.[22–24] The correlation analysis was performed to identify factors that had a significant correlation with the cab vibration. Figure 2 shows the signal collection analysis, the correlation coefficients between the cutting platform's various measurement points and the cab vibration, as well as the cab spectrum. The basic parameters of the acceleration sensors are presented in Table 1. The results proved that the vibration of the cutter had the highest correlation with the X and Y directions of the cab vibration, as indicated in the dashed boxes 1 and 2. The vibration of the swing ring was a secondary factor, as shown in the dashed boxes 3 and 4. Therefore, it was necessary to carry out vibration reduction for the cutter and swing ring systems. Moreover, from the three-directional spectrum diagram of the cab, it can be seen that the Y-direction vibration was most affected by the cutter vibration,

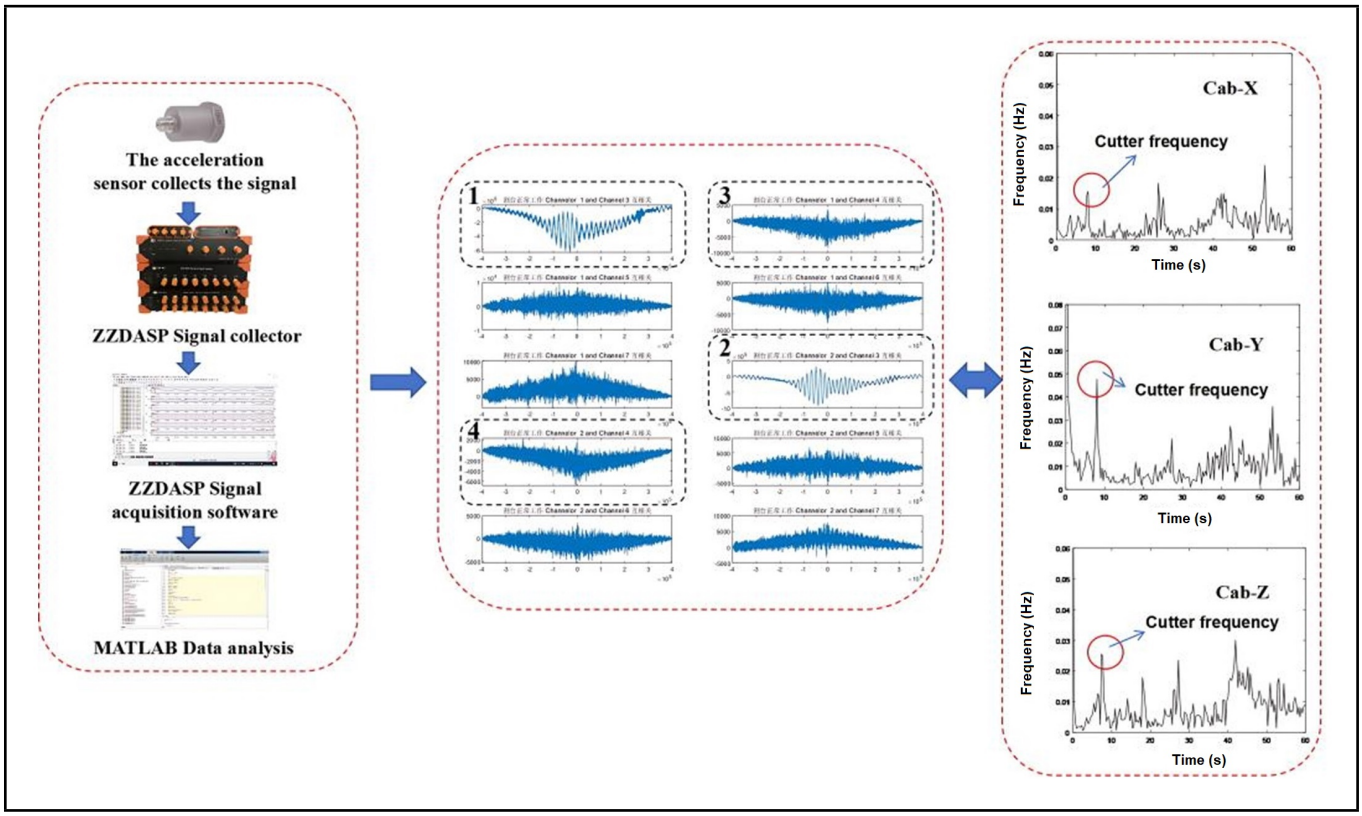

Figure 2. Schematic diagram of the vibration correlation between each measurement point of the cutting table and the cab.

while the Z-direction was relatively smaller.

The harvester will be accelerated to normal working conditions and make the cutter table run with the engine speed at 2400 r/min. The vibration acceleration of each channel was collected under this working condition, and the time domain graph of the vibration acceleration of the cutter is shown in Fig. 3a. The periodic acceleration value of the reciprocating motion of the cutter and the gap collision was mainly concentrated between -240 m/s^2 to 230 m/s^2. The vibration acceleration time-domain diagram of the pendulum ring system is shown in Fig. 3b, which was basically in the range of -15 m/s^2 to 15 m/s^2 with no influence of external noise. However, there was a non-periodic acceleration signal of 1000 m/s^2 in the cutter acceleration, which might be affected by noise. Therefore, the EEMD decomposition and reconstruction of this time-domain signal was carried out to eliminate the influence of irrelevant noise components on the vibration signal on the one hand and eliminate the aliasing modes in the vibration signal on the other hand.[25–27] The decomposed and reconstructed time-domain diagram is shown in Fig. 4.

2.2. Dynamic Modelling and Simulation of the Cutter and the Pendulum Ring System

The cutter and pendulum ring system consists of a spindle, pendulum ring, pendulum fork, pendulum shaft, pendulum arm, guide bar and cutting knife, etc. During the operation process, the spindle rotation drove the pendulum ring movement, and the pendulum ring movement drove the guide bar to push the cutting knife to carry out the reciprocating movement.[28–31] Its movement sketch is shown in Fig. 5 below.

It is known that the rotational speed of the drive spindle is ω. When the harvester cutter pendulum ring system is in motion, the inclined axis on the spindle (which can be considered as OB) makes a conical motion with an apex of O, and Point B is the intersection of the prolongation of the centre line of the inclined axis and the sprocket. Meanwhile, the angle between OB and the main axis is α, which is the pendulum angle of the pendulum ring system. Subsequently, the kinematic equation of Point B is established with the length of AB (L_{AB}), as the radius of gyration. The pendulum ring is driven by the rotation of the main axis to make its angle change, so in the kinetic model, the angular displacement driving the pendulum ring movement is expressed as β, i.e., the angle between the line connecting the upper and lower end points of the pendulum ring (CD) and the main axis OA, the kinematic equation of Point B is given in Eq. (1) below:

$$\begin{cases} x_B = L_{OB}\cos\alpha; \\ y_B = L_{AB}\sin\omega t; \\ z_B = L_{AB}\cos\omega t. \end{cases} \tag{1}$$

The kinematic equation of motion at point C of the pendulum ring is established as follows in Eq. (2):

$$\begin{cases} x_C = R\cos\beta; \\ y_C = 0; \\ z_C = R\sin\beta. \end{cases} \tag{2}$$

where R is the length of OC, which can be considered as the radius of the pendulum ring. According to the working principle of the pendulum ring mechanism, the two points C and D always move and change in the plane. According to the structural characteristics of the pendulum ring, it is known that OC and OB are perpendicular to each other, and according to the

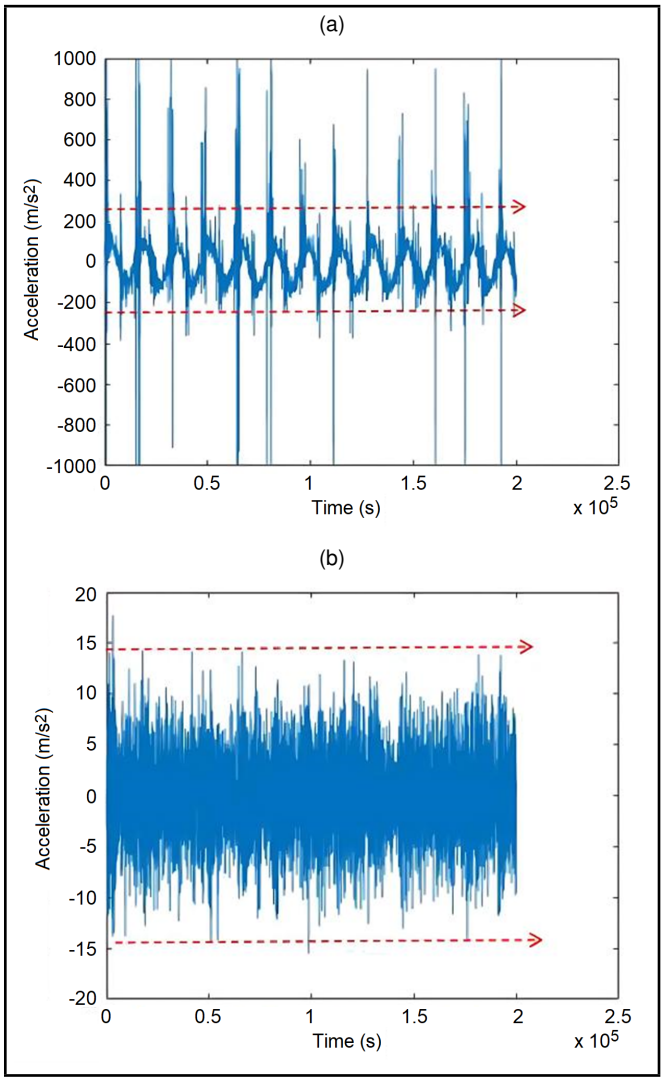

Figure 3. Time-domain diagram of the vibrational acceleration of the cutter and the pendulum ring under normal working conditions. (a) Cutter vibration time-domain, and (b) Pendulum ring vibration time-domain.

definition of vector product, assuming that there are two vector products of a and b, the product of the two vectors is shown in the following Eq. (3)

$$a \cdot b = a_x b_x + a_y b_y + a_z b_z = |a| \cdot |b| \cdot \cos\theta. \tag{3}$$

According to Eq. (3), the product of the two vectors OC and OB can be obtained as follows:

$$\overline{OB} \cdot \overline{OC} = \begin{bmatrix} x_B & y_B & z_B \end{bmatrix} \begin{bmatrix} x_C \\ y_C \\ z_C \end{bmatrix} = x_B x_C + y_B y_C + z_B z_C = 0. \tag{4}$$

Denote the displacement x_C at Point C of the pendulum ring as x_2, and according to Eq. (2), the velocity expression at Point C can be obtained as Eq. (5):

$$\dot{x}_2 = \dot{x}_C = -R\dot{\beta}\sin\beta. \tag{5}$$

Further derivation of the velocity Eq. (5) gives the acceleration Eq. (6) at Point C as:

$$\ddot{x}_2 = \ddot{x}_C = -R\left(\ddot{\beta}\sin\beta + \dot{\beta}^2\cos\beta\right). \tag{6}$$

Combined with Eq. (4), we can get Eq. (7):

$$\tan\beta = -\frac{1}{\tan\alpha\cos\omega t}. \tag{7}$$

Then the angular displacement can be expressed by Eq. (8) as:

$$\beta = \arctan\tan\beta = \arctan\left(-\frac{1}{\tan\alpha\cos\omega t}\right). \tag{8}$$

Derivation of Eq. (8) gives the angular velocity Eq. (9) as:

$$\dot{\beta} = \frac{\omega\tan\beta\tan\omega t}{1+\tan^2\beta}. \tag{9}$$

The angular acceleration Eq. (10) is obtained by further derivation of Eq. (9) as:

$$\ddot{\beta} = \omega\dot{\beta}\tan\omega t - 2\dot{\beta}^2\tan\beta + \omega^2\tan\beta + \frac{1+\tan^2\omega t}{1+\tan^2\beta}. \tag{10}$$

Suppose the length of the pendulum rod O_1E is L_{O1E}. The kinematic equation of Point E which drives the movement of the cutting knife in the pendulum ring is shown in Eq. (11):

$$\begin{cases} x_E = L_{O1E}\cos\beta; \\ y_E = 0; \\ z_E = L_{O1E}\sin\beta. \end{cases} \tag{11}$$

By deriving x_E in Eq. (11), we can obtain the velocity Eq. (12) at Point E as:

$$\dot{x}_E = -L_{O1E}\dot{\beta}\sin\beta. \tag{12}$$

Further derivation of Eq. (12) gives Eq. (13) for the acceleration at Point E as:

$$\ddot{x}_E = -L_{O1E}\left(\ddot{\beta}\sin\beta + \dot{\beta}^2\cos\beta\right). \tag{13}$$

The speed of the cutter during reciprocating movement is high. Therefore, under the action of inertial forces, the reciprocating travel of the cutting knife needs to be taken into account in the displacement of the cutter as a whole, except for point E of the pendulum. Set the reciprocating travel of the cutting knife as s. Since the reciprocating movement of the cutting knife is relatively fast, it can be regarded as a constant velocity motion. Knowing that the angular velocity of the drive mechanism is ω, the time taken by the cutting knife in one cycle of reciprocating motion is shown in Eq. (14):

$$t_1 = \frac{2\pi}{\omega}. \tag{14}$$

Then the expression for the dynamic real-time travel x_d of the cutting knife is shown in Eq. (15):

$$x_d = \frac{\omega s}{2\pi}t. \tag{15}$$

Set the displacement of the cutting knife as x_1, the expression for the displacement of the cutting knife is shown in Eq. (16):

$$x_1 = x_d + x_E = \frac{\omega s}{2\pi}t + L_{O1E}\cos\beta. \tag{16}$$

Firstly, the travelling distance s of the cutting knife is calculated. It is known that $\alpha = 20°$, $L_{O1E} = 160$ mm, the cutting knife's driving speed is 600 r/min in the normal working condition of the harvester, and the cutting knife is rigidly connected with Point E, so the travelling distance of Point E is

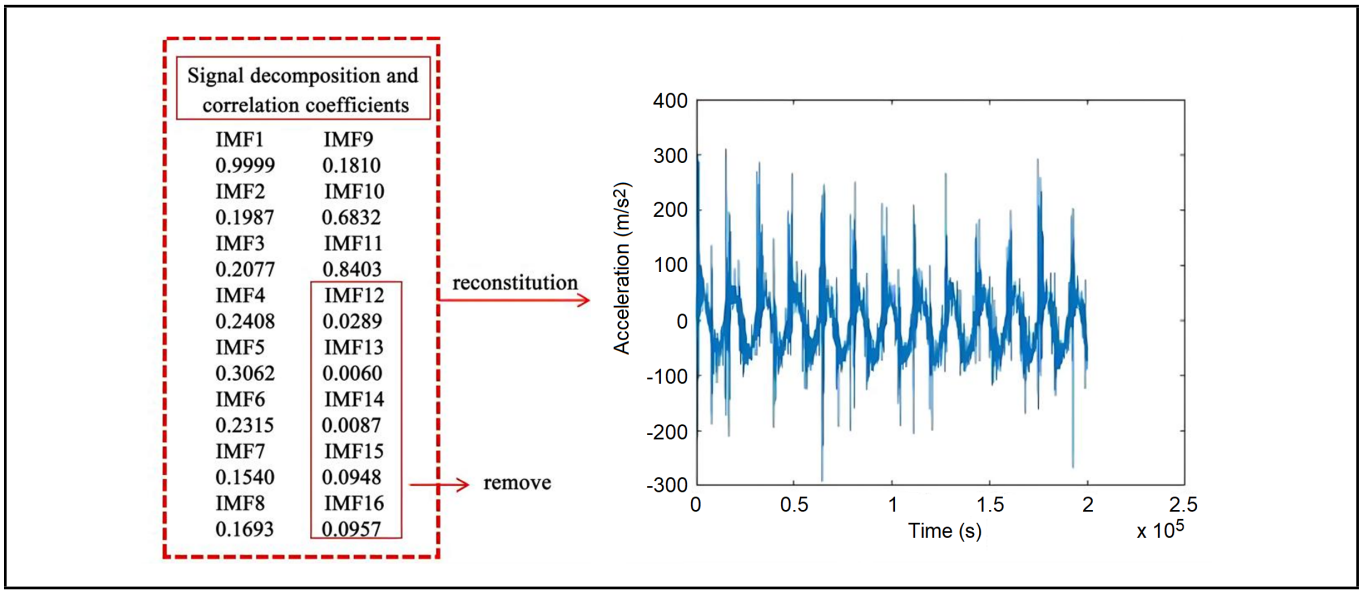

Figure 4. Time-domain diagram of vibration acceleration of the cutter after EEMD decomposition and reconstruction.

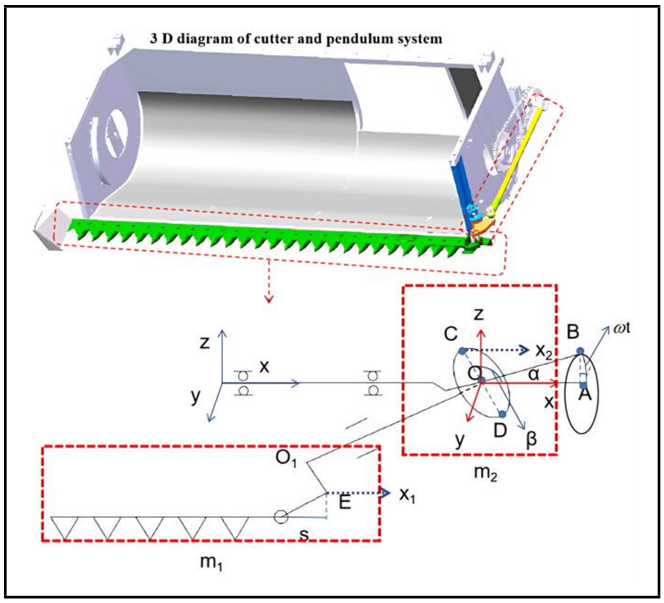

Figure 5. Simplified movement diagram of the cutter and pendulum ring system.

the travelling distance of the cutter. Therefore, the equation of s can be obtained, as shown in Eq. (17):

$$s = x_{E_{\max}} - x_{E_{\min}} = L_{O1E}\left(\cos\left(\alpha - \frac{\pi}{2}\right) - \cos\left(\alpha + \frac{\pi}{2}\right)\right). \tag{17}$$

Through calculation, s is 108 mm. Thus the expression for the dynamic travelling distance of the cutting knife is shown in Eq. (18):

$$x_d = \frac{\omega s}{2\pi}t = 17\omega t. \tag{18}$$

After deriving the derivative of the cutter displacement x_1, the cutter speed expression is obtained, as shown in Eq. (19):

$$\dot{x}_1 = 17\omega - L_{O1E}\dot{\beta}\sin\beta. \tag{19}$$

Then take the derivative of Eq. (19) and obtain the expression of the cutter acceleration, as shown in Eq. (20):

$$\ddot{x}_1 = -L_{O1E}\left(\ddot{\beta}\sin\beta + \dot{\beta}^2\cos\beta\right). \tag{20}$$

We combine Eqs. (8), (9), (10), and (20) and build the kinematic simulation model of the cutter in SIMULINK. The simulation model is shown in Fig. 6.

As shown in Fig. 6, the vibration acceleration of the cutter at the initial moment exceeds 200 m/s^2 and reaches 230 m/s^2. With the prolongation of the simulation time, the vibration acceleration gradually declines to about 220 m/s^2, and the simulation result is similar to the value of the acceleration of the cutter measured by the harvester accelerated to the normal working condition, which verifies the validity of the kinematic equation of the established cutter system.

Since the reciprocating motion of the cutter has a large impact on vibration, the vibration-damping design of the cutter system is required. Referring to the research on vibration damping of automobile and engineering machinery suspensions, etc., the cutter and pendulum ring system is simplified into a two-degree-of-freedom dynamics model,[32–34] as shown in Fig. 7.

Combined with Fig. 5, the cutter is simplified as a mass point m_1, and the pendulum ring is simplified as a mass point m_2. The connection between the cutter and the pendulum ring is simplified as a spring unit k_1 and a damping unit c_1, and the connection between the pendulum ring and the cutter drive mechanism is similarly simplified as a spring unit k_2 and a damping unit c_2. The kinetic equations of the cutter drive system are established according to Fig. 7, as shown in Eqs. (21) and (22)

$$m_1\ddot{x}_1 = k_1(x_2 - x_1) + c_1(\dot{x}_2 - \dot{x}_1) + f_2(t); \tag{21}$$

$$m_2\ddot{x}_2 = -k_1(x_2 - x_1) + c_1(\dot{x}_2 - \dot{x}_1) - k_2x_2 - c_2\dot{x}_2 + f_1(t). \tag{22}$$

The free vibration dynamics equation of the system is established, as shown in Eq. (23):

$$[M][\ddot{x}] = [K][x] + [C][\dot{x}] + [F]. \tag{23}$$

Based on the established dynamics model of the two-degree-of-freedom cutter and pendulum ring system, the specific form

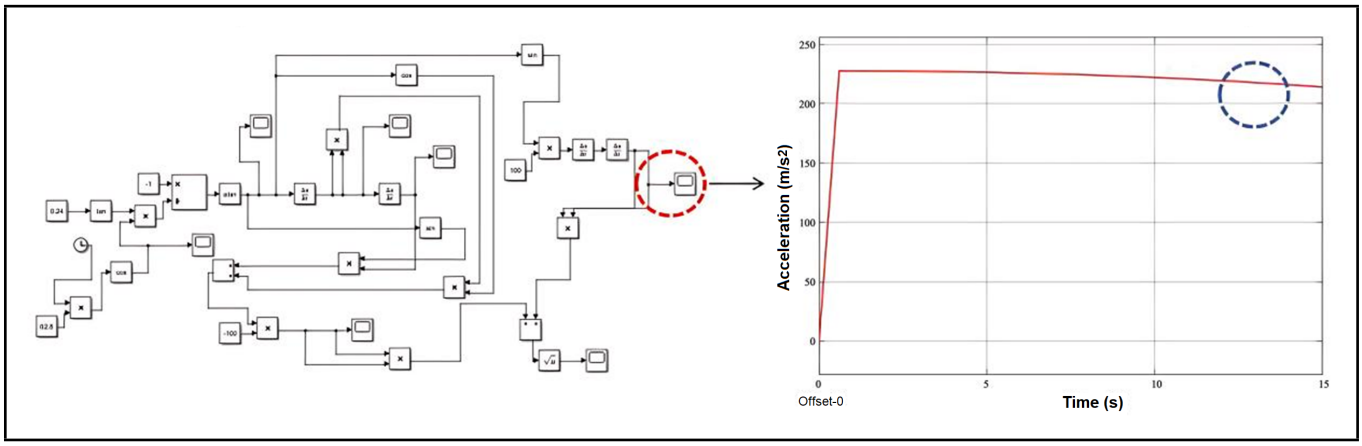

Figure 6. Kinematic simulation model of cutter and pendulum ring system and its results.

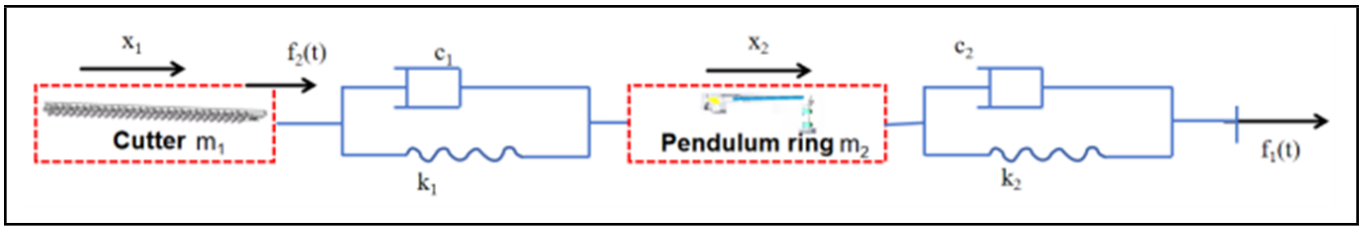

Figure 7. Two-degree-of-freedom dynamics model of the cutter and pendulum ring mechanism system.

of each matrix is derived, as shown in Eq. (24):

$$\begin{bmatrix} m_1 & \\ & m_2 \end{bmatrix} \begin{bmatrix} \ddot{x}_1 \\ \ddot{x}_2 \end{bmatrix} = \begin{bmatrix} -k_1 & k_1 \\ k_1 & -k_1-k_2 \end{bmatrix} \begin{bmatrix} x_1 \\ x_2 \end{bmatrix} + \begin{bmatrix} -c_1 & c_1 \\ -c_1 & c_1-c_2 \end{bmatrix} \begin{bmatrix} \dot{x}_1 \\ \dot{x}_2 \end{bmatrix} + \begin{bmatrix} f_2(t) \\ f_1(t) \end{bmatrix}. \quad (24)$$

Subsequently, a two-degree-of-freedom kinematic simulation model is built in MATLAB/SIMULINK, in which the cutter and the pendulum ring system are established as subsystems and encapsulated respectively. The simulation model is shown in Fig. 8, with the original parameters of the harvester: $m_1 = 20$ kg, $m_2 = 30$ kg, $k_1 = 10$, $k_2 = 30$, $c_1 = 10$, and $c_2 = 30$.

Through Eq. (24), we can get Eqs. (25) and (26) as follows:

$$\ddot{x}_1 = \frac{1}{m_1}\big(k_1x_2 - k_1x_1 + c_1\dot{x}_2 - c_1\dot{x}_1 + f_2(t)\big); \quad (25)$$

$$\ddot{x}_2 = \frac{1}{m_2}\big((-k_1-k_2)x_2 + k_1x_1 + (c_1-c_2)\dot{x}_2 - c_1\dot{x}_1 + f_1(t)\big). \quad (26)$$

When the harvester is accelerated to normal working conditions, the force driving the pendulum ring to move and the reciprocating motion of the cutter can be considered as a periodic signal, and the signal is shown in Eq. (27):

$$f(t) = \begin{cases} T & t \in [0, t_1]; \\ -T & t \in [t_1, t_2]. \end{cases} \quad (27)$$

After building the two-degree-of-freedom kinematic simulation model, the cuckoo search algorithm is used to search for the optimal values of stiffness and damping of the cutter system.

2.3. Using the Cuckoo Search Algorithm to Find the Optimal Values of Stiffness and Damping of the Cutter System

2.3.1. Establishment of the Objective Function

To reduce the vibration of the cutter system, we need to change the stiffness and damping value of the system, but the displacement of the system will change. Therefore, a target function is established based on the root mean square (RMS) value of vibration acceleration and the RMS value of displacement.[35,36] When it comes to the allocation of weights, given that the focus of this study lies in the impact of the vibrations generated by the cutter's motion on the cab, ideally, a target function that is solely related to acceleration should be formulated. However, the reciprocating motion of the cutter also involves significant displacement changes, which have a certain impact on the vibration. Taking into account both factors, acceleration accounts for $3/4$ and displacement accounts for $1/4$ of the weight. The target function is shown in Eq. (28):

$$\min J = \frac{3}{4}\sigma_a^2 + \frac{1}{4}\sigma_x^2; \quad (28)$$

where σ_a represents the root mean square value of the vibration acceleration of the cutter system and σ_x represents the root mean square value of the displacement of the cutter system.

2.3.2. Establishment of Constraints

The constraints on the stiffness of the cutter system can be calculated from the bias frequency n as:

$$k = (2\pi n)^2 m_1. \quad (29)$$

Set the upper and lower limits of the bias frequency n according to the bias frequency value table as:

$$n \in [0.1, 0.2]. \quad (30)$$

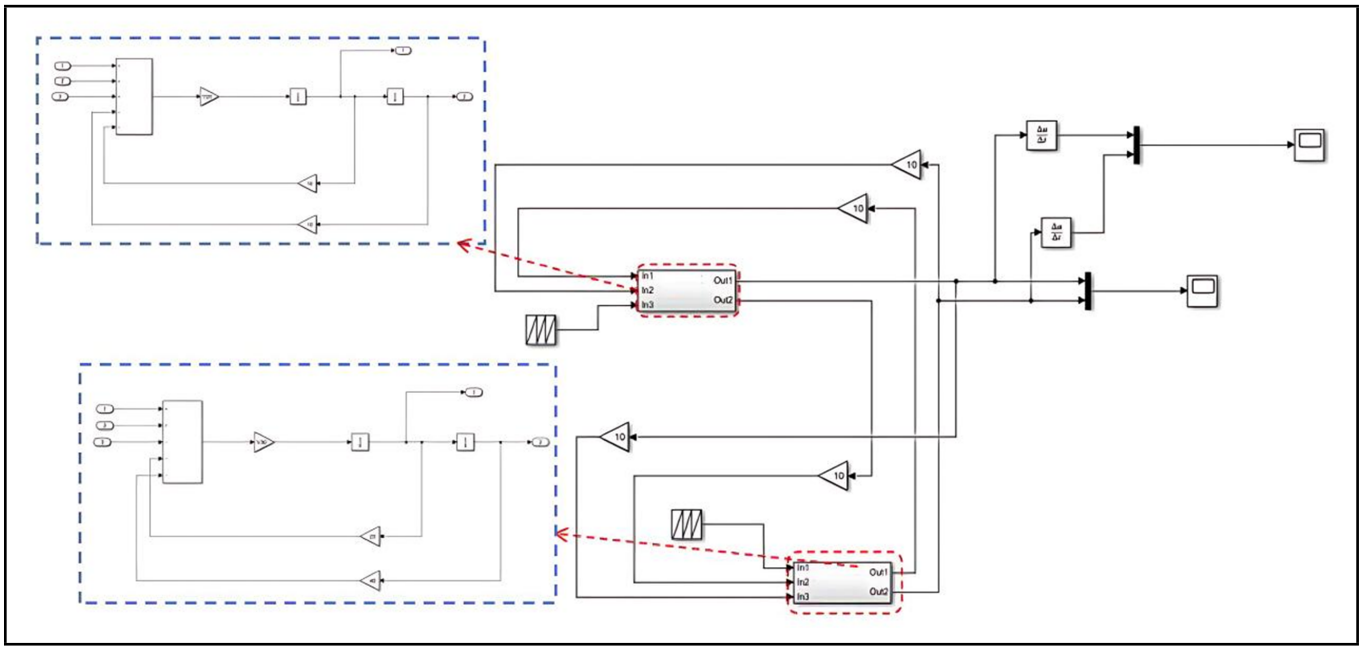

Figure 8. Two-degree-of-freedom kinematic simulation model of the cutter and pendulum ring mechanism system.

The upper and lower limits of stiffness can be calculated as:

$$7.8 < k < 31.5. \tag{31}$$

The damping coefficient of the shock absorber can be calculated from the relative damping coefficient of the suspension. The formula is:

$$c = 2\sqrt{km_1\varphi}. \tag{32}$$

In this paper, the upper and lower damping limits are obtained by taking the relative damping coefficients φ between 0.25 and 0.35, as follows:

$$12.5 < c < 30. \tag{33}$$

2.3.3. Cuckoo Search Algorithm

The cuckoo search algorithm effectively solves the optimisation problem by simulating the cuckoo's parasitic brood habit.[37,38] It employs an iterative approach, where the cuckoos randomly fly from one nest to another to seek out the nest with the highest probability of safely hatching the offspring. If the host finds a cuckoo egg, it will throw it away or abandon the nest. The cuckoo algorithm uses Levy flight to realize the iteration of the cuckoo flying from one nest to another, as shown in the following Eq. (34):

$$d_{i+1}^e = d_i^e + \tau \times \frac{|u|}{v^{1/\gamma}} \times (d_{best} - d_i^e); \tag{34}$$

where i is the number of iterations, $e = 1, 2, \ldots$ is the search step size, u and v are random matrices based on normal distribution, γ is a constant similar to the diffusion coefficient, and $d_{best} - d_i^e$ represents the location of a random bird's nest, as shown in Eq. (35):

$$|u \sim N(0, \sigma_u^2), \quad v \sim N(0, \sigma_v^2)|. \tag{35}$$

Among them, the variances of u and v are shown in Eq. (36), where $\lambda = 1.5$:

$$\sigma_u = \left(\frac{\Gamma(1+\lambda) \times \sin(\pi \times \lambda/2)}{\Gamma\left(\frac{1+\lambda}{2}\right) \times \lambda \times 2^{\frac{\lambda-1}{2}}} \right), \quad \sigma_v = 1; \tag{36}$$

Table 2. Four working conditions of simulation parameter settings.

Working conditions	m_1 (kg)	m_2 (kg)	k_1 (N/m)	k_2 (N/m)	c_1 (Ns/m)	c_2 (Ns/m)
1	20	30	10	30	10	30
2	20	30	20	30	25	30
3	20	30	10	30	12.5	30
4	20	30	17	30	29	30

where Γ is the Gamma function.

After each iteration, the cuckoo egg is in danger of being discovered by the host, and the probability of discovery is p. After the position is changed by Levy flight, a number ranging from 0 to 1 is generated and compared with the probability p of finding the egg.

If $rand < p$, the cuckoo will fly to a random nest and iterate again. To speed up the convergence of the algorithm, the iteration algorithm after the cuckoo egg is discovered is improved. The cuckoo does not fly to a random position but continues to iterate to the current global optimal d_{best}, as shown in Eq. (37):

$$d_{i+1}^e = d_i^e + rand(d_{best} - d_i^e). \tag{37}$$

If $rand > p$, the optimal solution of the previous generation is retained, and the whole process can be represented by the following flow Fig. 9.

2.3.4. Simulation Results and Discussion

Parameter optimisation of the cutter system is carried out by applying the cuckoo search algorithm under the set constraints to obtain the optimised stiffness values and damping values ($k_1 = 20$, $c_1 = 25$).The simulation analysis of the vibration system before and after the optimisation is then carried out. The simulation parameters are set to the following four conditions, with condition 2 being the optimisation condition and the remaining three conditions being the comparison conditions, as shown in Table 2.

The simulation results of the four working conditions are shown in Fig. 10, where the red line represents the cutter and the blue line represents the pendulum ring.

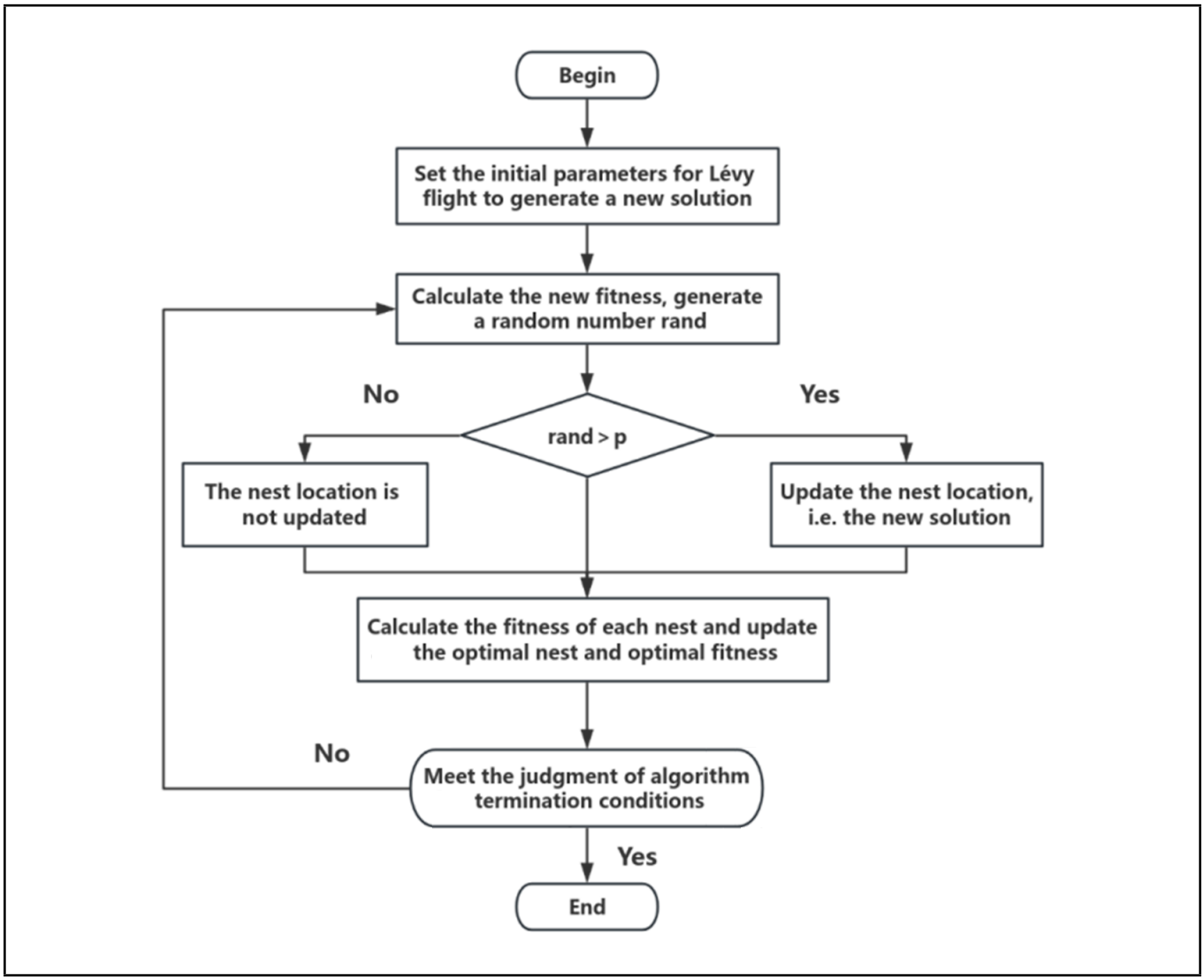

Figure 9. Flowchart of the cuckoo algorithm to search for the best value of stiffness and damping of the cutter system.

In Fig. 10(a), in the initial stage of working condition 1, the acceleration of the pendulum ring and the cutter suddenly increased to the peak value. The acceleration amplitude of the cutter is 260 m/s^2, and the acceleration amplitude of the pendulum ring is 80 m/s^2. With the prolongation of the working time, the acceleration becomes smoother, the amplitude of vibration acceleration of the cutter becomes -240 m/s^2 to 220 m/s^2, and the amplitude of vibration acceleration of the pendulum ring becomes -13 m/s^2 to 15 m/s^2. The simulation results of the simplified two-degree-of-freedom dynamics model are similar to the measured vibration acceleration values under the original parameters of the harvester, which proves that the model of the cutter and pendulum ring system meets the design requirements.

In Fig. 10(b), in the beginning stage, the displacement amplitude of the pendulum ring and the cutter suddenly increases, with the peak displacement of the pendulum ring increasing to 13 cm and the peak displacement of the cutter increasing to about 20 cm. This is due to the sudden load force applied to the cutter and the pendulum ring, prompting them to change from static to dynamic, and the duration of this state is relatively short, which can be considered to be caused by the error. With the prolongation of the working time, both the pendulum ring and the displacement amplitude of the cutter are reduced, in which the amplitude of the displacement change of the pendulum ring is about 10 cm, the displacement change of the cutter is reduced to -5 cm to 8 cm. Due to the reciprocating movement of the cutter, it can be considered that the displacement amplitude of the pendulum ring is about 6.5 cm, and the displacement change of the pendulum ring is less than the displacement change of the cutter.

In Fig. 10(c), the vibration acceleration change of the cutter under working condition 2 is more obvious compared with working condition 1. The vibration acceleration amplitude in the positive zone decreases to 180 m/s^2 during the stable operation stage of the cutter, and the vibration acceleration amplitude in the negative zone is mostly in the range of -205 m/s^2, which is smaller than that of working condition 1 overall. It indicates that the increase of stiffness and damping at the same time plays a certain inhibiting effect on the vibration acceleration of the cutter.

In Fig. 10(d), the displacement of the cutter and the pendulum ring is smoother with less beating during the smooth phase of the cutter operation.

In Fig. 10(e), the amplitude of the vibration acceleration of the cutter in the negative zone increased compared to working condition 2, mostly at -240 m/s^2.

In Fig. 10(f), the displacement amplitude of both the pendu-

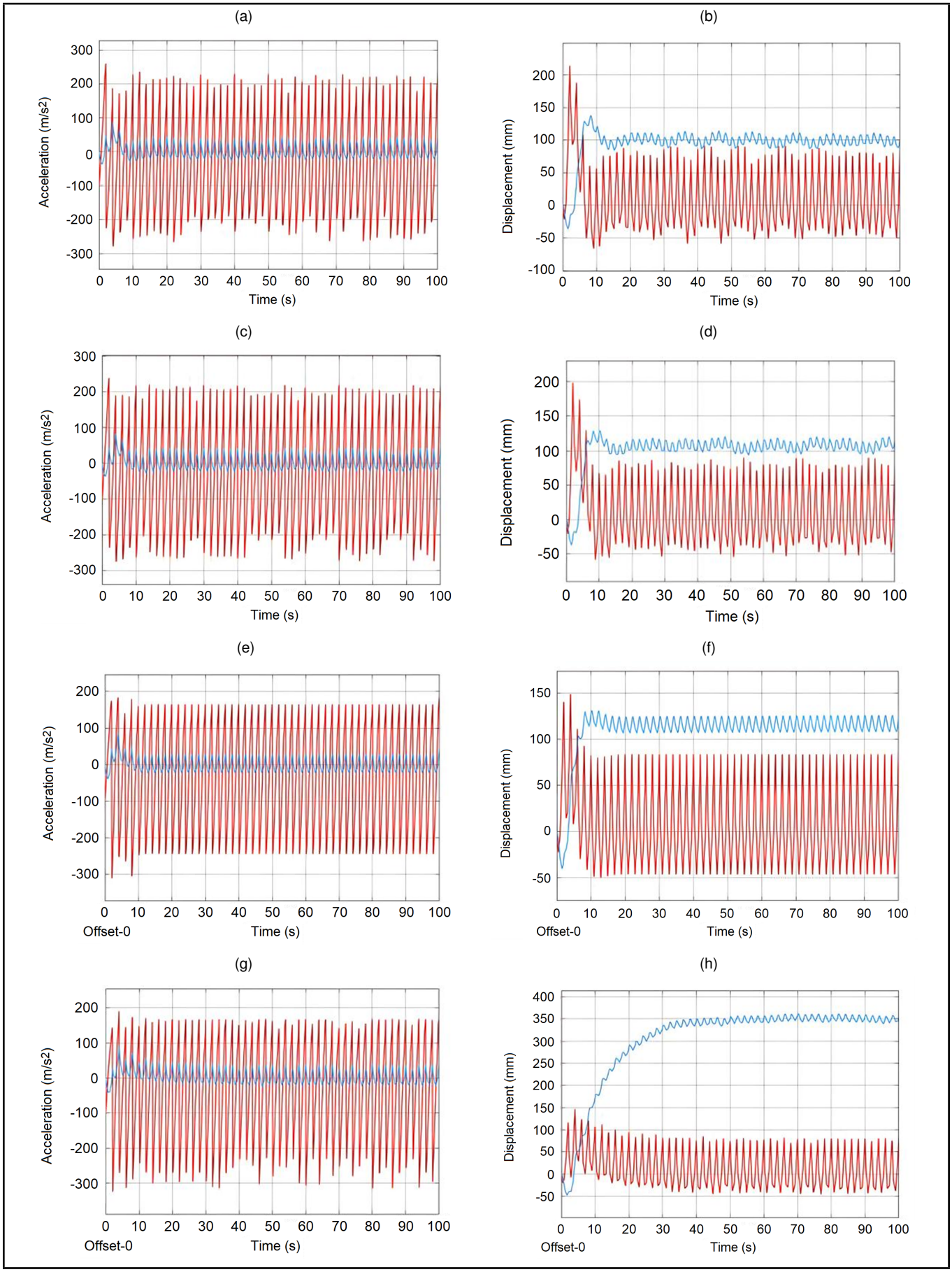

Figure 10. Simulation results of vibration acceleration and displacement of cutter and pendulum ring system under four working conditions, (a) Vibration acceleration signal of working condition 1, (b) Displacement change in working condition 1, (c) Vibration acceleration signal of working condition 2, (d) Displacement change in working condition 2, (e) Vibration acceleration signal of working condition 3, (f) Displacement change in working condition 3, (g) Vibration acceleration signal of working condition 4, and (h) Displacement change in working condition 4.

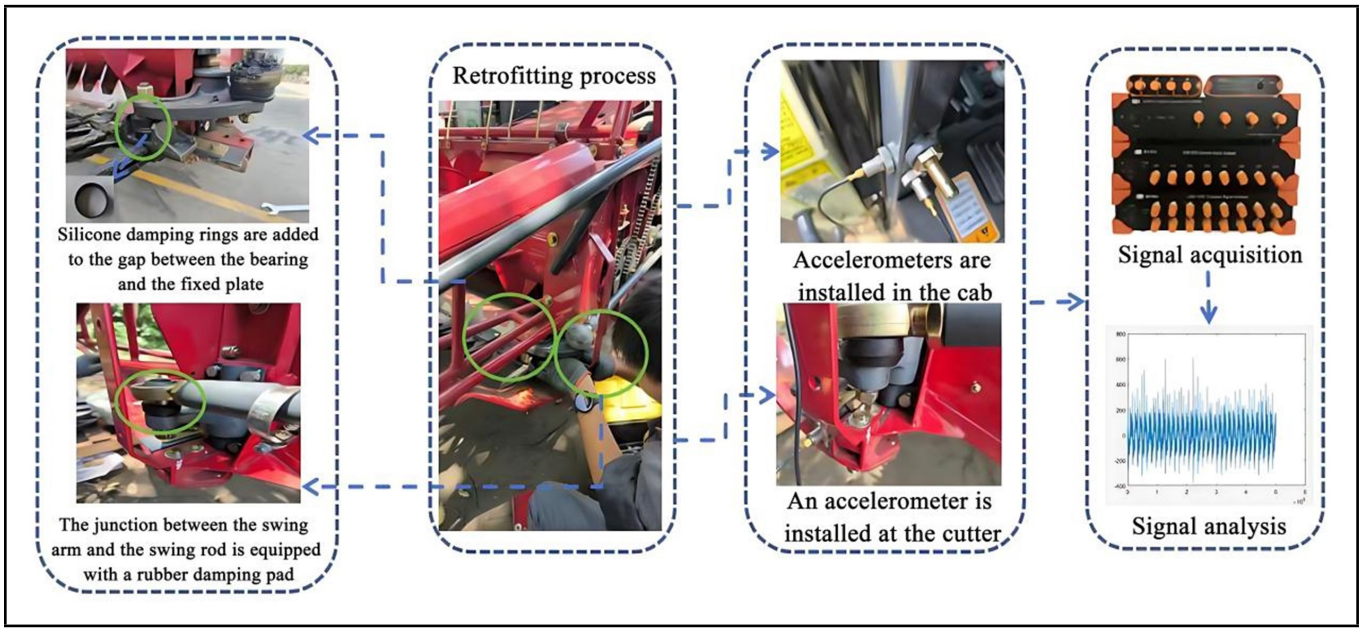

Figure 11. The process of adding POM bearing bushing and damping rubber and vibration measurement after system improvement.

lum ring and the cutter increases, increasing the instability of the cutter system.

In Fig. 10(g), the acceleration of the pendulum ring does not change significantly, but the negative interval of the cutter acceleration increases significantly in comparison to working condition 2, up to more than -300 m/s^2.

In Fig. 10(h), the reciprocating displacement of the cutter does not change much, but the displacement of the pendulum ring increases dramatically from the initial 100 mm to 350 mm, so the increase in the swinging amplitude of the pendulum ring mechanism tends to accelerate the wear and tear of the parts. In summary, the combination of the parameters in working condition 2 is more conducive to reducing the vibration of the harvester's cutter system.

3. TEST RESULTS AND DISCUSSION

The optimal combination of the cutter system's stiffness and damping parameters, which is obtained from the above simulation, is adopted for the experimental verification of the vibration - damping performance of the harvester cutter system, and the optimal combination of parameters is ($k_1 = 20$, $c_1 = 25$). Therefore, the stiffness and damping coefficients of the system are adjusted to the optimal parameter combinations by adding POM bearing bushings at the gap between the bearing driving the reciprocating cutter and its fixing plate, and by adding rubber damping pads at the connection between the pendulum arm and the pendulum bar. The process of adding POM bearing bushings and vibration-damping rubber and the vibration measurement after the system improvement are shown in Fig. 11.

Firstly, the vibration acceleration of the cutter is collected for analysis, and the time-domain diagram of the vibration acceleration of the improved cutter is shown in Fig. 12(a). The time-domain diagram of the vibration acceleration of the original cutter is shown in Fig. 12(b).

Comparing Figs. 12(a) and 12(b), it can be seen that the vibration acceleration of the cutter is reduced, and the amplitude of the acceleration signal of the improved cutter system is reduced as well, with the negative peak value around -200 m/s^2 and the positive peak value below 200 m/s^2. To better characterise the size of the vibration signals, the RMS values are calculated respectively. The original model is 93.86, and the improved model is 86.04, which is 8.4% lower which further illustrates that the vibration of the cutter system decreases after the improvement.

In the simulation results under conditions 1 and 2, the vibration decreases by about 10%, while in the test results, and the vibration decreases by 8.4%, with an error of 1.6%. The theoretical value decreases more because the simulation condition is ideal and free from external interference. However, during the actual test, external interference is inevitable. This leads to a slightly lower vibration reduction percentage. Nevertheless, the result is still within the error range, which validates the effectiveness of the simulation.

The ultimate goal of cutter damping is to reduce the vibration of the cab, and this study measures and compares the magnitude of the vibration acceleration of the cab before and after the improvement. The time-domain diagram of the vibration of the cab in the Y-direction before and after the improvement is shown in Fig. 13.

By comparing Figs. 13(a) with 13(b), the Y-direction vibration acceleration of the cab has decreased significantly, with the RMS value changing from the original 0.31 to 0.27, a reduction of 12.9%. It can be concluded that the vibration of the cab has been improved.

4. CONCLUSIONS

In this paper, vibration signal test and analysis were carried out on various parts of the combine harvester's cutting table and cab. Additionally, the kinematic equations were derived, and the two-degree-of-freedom dynamic model was simplified for the cutter pendulum ring system. Subsequently, the parameters of the cutter system were optimized based on the cuckoo search algorithm, leading to the following conclusions:

(1) Under the normal working conditions of the combined harvester, the correlation between the vibration of the cutter and the cab was the largest, followed by the pendulum

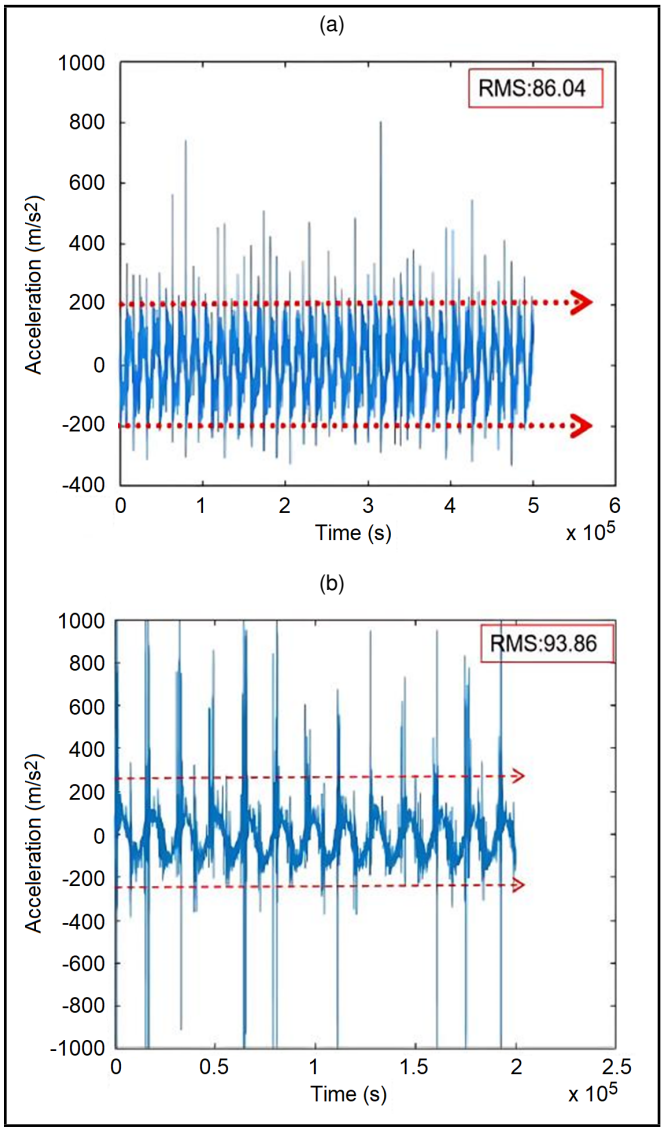

Figure 12. Time-domain diagram of the vibration acceleration of the improved and original cutter. (a) Time-domain diagram of the vibration of the improved cutter, and (b) Time-domain diagram of the vibration of the original.

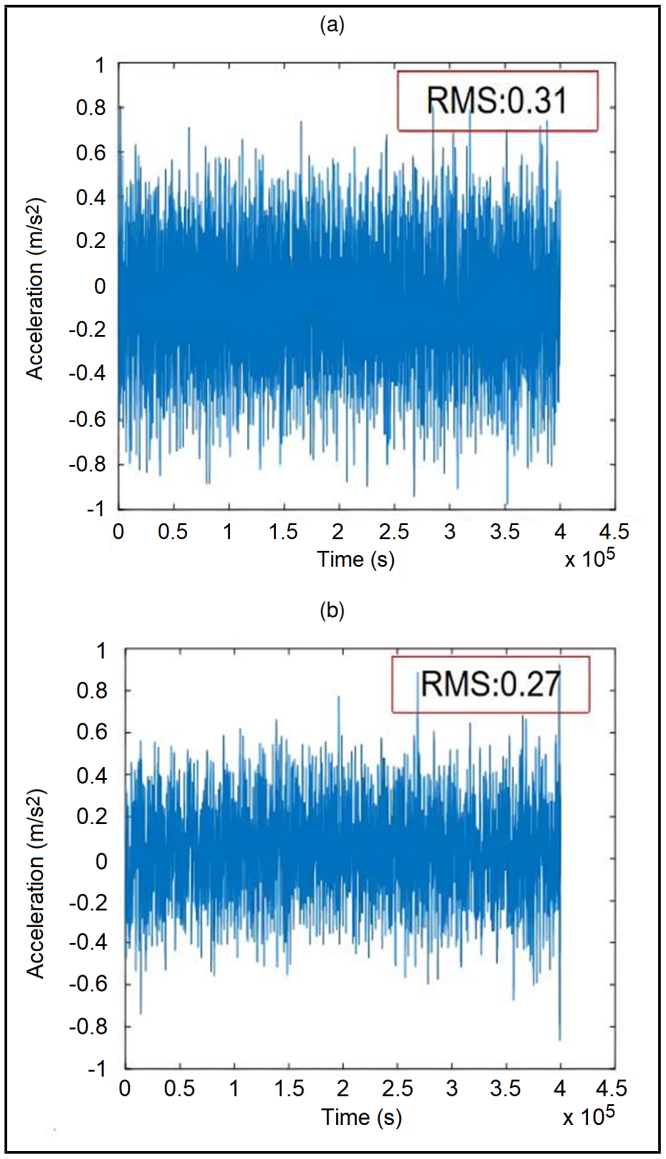

Figure 13. Comparison of vibration time domain diagrams in the Y direction of the cab before and after improvement. (a) Y direction vibration acceleration in the original model, and (b) Improved cab Y-direction vibration acceleration.

ring system. The vibration acceleration of the cutter was obviously stronger than that of the pendulum ring, the vibration acceleration of the cutter was about -240 m/s^2 to 220 m/s^2, and the vibration acceleration of the pendulum ring was about -13 m/s^2 to 15 m/s^2.

(2) The kinematic equations of the cutter and its pendulum ring system were established and simplified into a two-degree-of-freedom dynamics model, and a SIMULINK simulation model was constructed to obtain the vibration and acceleration simulation diagrams of the cutter system under the four working conditions. The results showed that the simulation results of working condition 1 were similar to the experimental measurements under the original parameters of the harvester, which verified the correctness of the simplified model and provided a basis for the subsequent vibration damping of the cutter system.

(3) The optimal damping and stiffness parameters of the system were solved by the cuckoo search algorithm. According to the optimal combination of parameters, the simulation results showed that when the stiffness and damping coefficients were $k_1 = 20$ and $c_1 = 25$, the vibration of the cutter was reduced significantly. Three comparative working conditions were set up for the comparative analysis, and the vibration of the cutter was reduced by about 10% compared with the original working condition.

(4) Finally, by installing POM bearing sleeves and rubber dampers on the cutter system, the system's stiffness and damping were adjusted to near the optimal parameters and then tested. The results indicated that the vibration RMS values of both the cutter and the cab were reduced. Specifically, the Y-direction vibration decreased by 12.9%. This demonstrated that when the stiffness and damping coefficients are set to $k_1 = 20$ and $c_1 = 25$, the vibrations of the cutter and cab are significantly improved, enhancing the driver's comfort. This method also provided a new approach for the vibration reduction optimisation of other working components of the harvester, including the dynamics of the threshing drum of a harvester, the kinematic equations of the reciprocating motion of a vibrating screen, and the establishment and simu-

lation optimisation of the cab suspension dynamic model. By adopting some effective vibration reduction measures, the vibration of the harvester can be reduced in all aspects.

FUNDING

The work was supported by the National Natural Science Foundation of China (No. 52275251), the Major scientific and technological innovation projects in Shandong Province (No. 2019JZZYO10729)

REFERENCES

[1] Li, Y., Xu, L. Z., Gao, Z. P., Lu, E., and Li, Y. M. Effect of vibration on rapeseed header loss and optimization of header Frame, *Transactions of the ASABE*, **64**, 1247–1258, (2021). https://doi.org/10.13031/trans.13299

[2] Yu, Z. W., Li, Y. M., Xu, L. Z., Du, X. X., and Ji, K. Z. Unbalance variation after assembly and double-speed influence coefficient method in the threshing drum, *International Journal of Agricultural and Biological Engineering*, **16**, 1–10, (2023). https://doi.org/10.25165/j.ijabe.20231606.7651

[3] Zheng, G. Q., Li, Y. M., Ji K. Z., Liang, Z. W., and Ma, X. Vibration analysis and structural optimization of cutting rack of millet combined harvester (in Chinese), *Agricultural Mechanization Research*, **46**, 41–45, (2024). https://doi.org/10.13427/j.cnki.njyi.2024.01.002

[4] Pang, J., Li, Y., Ji, J. T., and Xu, L. Z. Vibration excitation identification and control of the cutter of a combine harvester using triaxial accelerometers and partial coherence sorting, *Biosystems Engineering*, **185**, 25–34, (2019). https://doi.org/10.1016/j.biosystemseng.2019.02.013

[5] Wang, B. Z., Chen, S. R., Wang, G. Q., Tang, Z., and Ding, H. T. Damping optimization method of combine harvester frame undergoing multi-source excitation, *Agriculture*, **14**, 815, (2024). https://doi.org/10.3390/agriculture14060815

[6] Gao, Y. Y., Yang, Y. F., Hu, Y. Y., Han, X., Feng, K. Y., Li, P. Y., Wei, X. H., and Zhai, C. Y. Analysis of vibration characteristics of tractor-rotary cultivator combination based on time domain and frequency domain, *Agriculture*, **14**, 1139, (2024). https://doi.org/10.3390/agriculture14071139

[7] Chen, S. R., Zhou, Y. P., Tang, Z., and Lu, S. N. Modal vibration response of rice combine harvester frame under multi-source excitation, *Biosystems Engineering*, **194**, 177–195, (2020). https://doi.org/10.1016/j.biosystemseng.2020.04.002

[8] Wang, X. Z., Hong, T. Y., Fang, W. Q., and Chen, X. Y. Optimized design for vibration reduction in a residual film recovery machine frame based on modal analysis, *Agriculture*, **14**, 543, (2024). https://doi.org/10.3390/agriculture14040543

[9] Liu, Y., Li, Z. K., and Wu, H. T. Design and analysis of speed parameters for reciprocating cutter optimization based on ADAMS (in Chinese), *Agricultural Mechanization Research*, **33**, 42–45, (2011). https://doi.org/10.13427/j.cnki.njyi.2011.08.042

[10] Ran, J. H., Mu, S. L., and Li, H. T. Design and test of rape co-harvester (in Chinese), *Transactions of the Chinese Society of Agricultural Engineering*, **36** (09), 17–25, (2020). https://doi.org/10.11975/j.issn.1002-6819.2020.09.002

[11] Li, J. F., Liu, Q. X., and Zhang, K. X. Grain combine harvester cutter and complete machine ride comfort simulation analysis based on ADAMS (in Chinese), *China Agricultural Science and Technology Herald*, **21**, 62–69, (2019). https://doi.org/10.13304/j.nykjdb.2018.0075

[12] Wang, M., and Yan, C. Y. Study on vibration control method of crawler combine (in Chinese), *Agricultural Mechanization Research*, **46**, 75–79, (2024). https://doi.org/10.13427/j.cnki.njyi.2024.08.021

[13] Pang, J. *Vibration source-Response analysis and transmission main path identification of crawler grain combine* (in Chinese), Jiangsu University, Jiangsu China, (2019). https://doi.org/10.27170/d.cnki.gjsuu.2019.000020

[14] Zhang, X. L. and Peng, K. D. Vibration control method for a crawler-type combine harvester, *International Journal of Agricultural and Biological Engineering*, **30**, 873–882, (2018). https://doi.org/10.9755/ejfa.2018.v30.i10.1831

[15] Deng, X., Li, S. P., and Wang, M. P. Analysis of the vibration performance of the sugarcane harvester cutter (in Chinese), *Agricultural Mechanization Research*, **41** (01), 59–65, (2019). https://doi.org/10.13427/j.cnki.njyi.2019.01.010

[16] Yılmaz, D. and Gökduman, M. E. Development of a measurement system for noise and vibration of combine harvester, *International Journal of Agricultural and Biological Engineering*, **13**, 104–108, (2020). https://doi.org/10.25165/j.ijabe.20201306.5554

[17] Bhandari, S. K., and Jotautiene, E. Vibration analysis of a roller bearing condition used in a tangential threshing drum of a combine harvester for the smooth and continuous performance of agricultural crop harvesting, *Agriculture*, **12**, 1969, (2022). https://doi.org/10.3390/agriculture12111969

[18] Titova, L. L., Chernik, Y. M., Gumenyuk, Y. O., and Korobko, M. M. Research of Daubechies wavelet spectrum of vibroacoustic signals for diagnostic of diesel engines of combine harvesters, *IOP Conference Series: Earth and Environmental Science*, **548**, 032030, (2020). https://doi.org/10.1088/1755-1315/548/3/032030

[19] Wang, H. X., Li, G. Q., Dong, G. Y., and Wang, X. Cross-correlation analysis of the vibration characteristics of the RV reducer (in Chinese), *Automation and Instrumentation*, **38**, 91–94, (2023). https://doi.org/j.cnki.1001-9944.2023.06.019

[20] Jing, T., Tang, Z., Ding, Z., Liang, Y. Q., Fang, M., and Wang, T. Paddy soil compaction effect undergoing multi-dimensional dynamic load of combine harvester crawler, *Agriculture*, **14**, 202, (2024). https://doi.org/10.3390/agriculture14020202

[21] Que, K. X., Zhuang, X. B., Shi, Y. Y., Ding, Z. X., Tang, Z., Jing, T. T., Gao, Y. L., Wang, B. Z., and Yu, Y. Winding characteristics and signal characterization of roller during threshing of mature rice, *Agriculture*, **14**, 2332, (2024). https://doi.org/10.3390/agriculture14122332

[22] Nishat, T. R., Kim, C. H., and Kim, J. M. Bearing fault classification using ensemble empirical mode decomposition and convolutional neural network, *Electronic*, **10**, 1248, (2021). https://doi.org/10.3390/electronics10111248

[23] Ding, Z. X., Tang, Z., Zhang, B., and Ding, Z. Vibration response of metal plate and shell structure under multi-source excitation with welding and bolt connection, *Agriculture*, **14**, 816, (2024). https://doi.org/10.3390/agriculture14060816

[24] Liang, Z. W., Qin, Y. Q., and Su, Z. Establishment of a feeding rate prediction model for combine harvesters, *Agriculture*, **14**, 589, (2024). https://doi.org/10.3390/agriculture14040589

[25] Tanvir, A. S., and Jang, W. H. EEMD assisted supervised learning for the fault diagnosis of BLDC motor using vibration signal, *Journal of Mechanical Science and Technology*, **34**, 1–10, (2020). https://doi.org/10.1007/s12206-020-2208-7

[26] Li, H., Liu, T., Wu, X., and Li, S. B. Research on test bench bearing fault diagnosis of improved EEMD based on improved adaptive resonance technology, *Measurement*, **185**, (2021). https://doi.org/10.1016/j.measurement.2021.109986

[27] Tian, J., Wang, Y. J., Liu, L. L., Zhang, F. L., and Ai, Y. T. Extraction of rolling bearing fault features based on Birge-Massart threshold noise reduction, EEMD and spectral cliff degree (in Chinese), *Journal of Aviation Dynamics*, **34** (06), 1399–1408, (2019). https://doi.org/10.13224/j.cnki.jasp.2019.06.023

[28] Xie, F. *Study on digital design of cutting mechanism of small combine harvester* (in Chinese), Xihua University, Sichuan China, (2015).

[29] Zhao, H. Q. *Dynamics simulation and finite element analysis of the pendulum ring mechanism* (in Chinese), Hunan University, Hunan China, (2011).

[30] Shi, Z. L., Tang, X. P., Yan, J. S., Zhang, X. J., and Zhou, W. Q. Simulation and analysis of rigid and flexible coupling of swing ring mechanism of reciprocating cutting device (in Chinese), *Agricultural Research in Arid Areas*, **36**, 292–296, (2018). https://doi.org/10.7606/j.issn.1000-7601.2018.03.43

[31] Widner, A., Tihanyi, V., and Tettamanti, T. Framework for vehicle dynamics model validation, *IEEE Access*, **10**, 35422–35436, (2022). https://doi.org/10.1109/ACCESS.2022.3157904

[32] Čerškus, A., Uşinskis, V., Šešok, N., Iljin, I., and Bučinskas, V. Optimization of damping in a semi-active car suspension system with various locations of masses, *Applied Sciences*, **13**, 5371, (2023). https://doi.org/10.3390/app13095371

[33] Yun, S., Lee, J., Jang, W., Kim, D., Choi, M., and Chung, J. Dynamic modeling and analysis of a driving passenger vehicle, *Applied Sciences*, **13**, 5903, (2023). https://doi.org/10.3390/app13105903

[34] Xue, P., Ren, P. F., Zhang, H. Y., and Wang, Y. Q. Control parameter setting of intelligent vehicle drive motor based on cuckoo algorithm (in Chinese), *Journal of Henan Institute of Engineering (Natural Science Edition)*, **33**, 50–53, (2021). https://doi.org/10.16203/j.cnki.41-1397/n.2021.03.010

[35] Chen, J. T. and Xiong, Y. Multi-strategy adaptive cuckoo search algorithm for numerical optimization, *Artificial Intelligence Review*, **56**, 2031–2055, (2022). https://doi.org/10.1007/s10462-022-10222-4

[36] Su, Z. *Study on adaptive control method of variable diameter drum and threshing device of rice combined harvester* (in Chinese), Jiangsu University, Jiangsu China, (2020). https://doi.org/10.27170/d.cnki.gjsuu.2020.002315

[37] Zhang, Z. L. *Study on the optimization of automobile suspension parameters based on ride comfort* (in Chinese), Lanzhou Jiaotong University, Gansu China, (2023). https://doi.org/10.27205/d.cnki.gltec.2023.000311

[38] Meryem, K. A., Musa, A., and Mustafa, E. Investigation of temperature effect on the optimal weight design of steel truss bridges using Cuckoo Search Algorithm, *Structures*, **59**, 105819, (2024). https://doi.org/10.1016/j.istruc.2023.105819